In vivo selection for corrected ß-globin alleles after CRISPR/Cas9 editing in human sickle hematopoietic stem cells enhances therapeutic potential

Wendy Magis[1]*, Mark A. DeWitt[2]*, Stacia K. Wyman[2], Jonathan T. Vu[2], Seok-Jin Heo[1], Shirley J Shao[2], Fiona Hennig[1], Zulema G. Romero[3], Beatriz Campo-Fernandez[3], Matthew McNeill[4], Garrett R. Rettig[4], Yongming Sun[5], Patrick J. Lau[5], Yu Wang[5], Mark A. Behlke[4], Donald B. Kohn[3], Dario Boffelli[1], Mark C. Walters[1,6]**, Jacob E. Corn[2]**, David I.K. Martin[1]**

[1]Children's Hospital Oakland Research Institute, UCSF Benioff Children's Hospital Oakland, Oakland, CA 94609, USA

[2]Innovative Genomics Institute, University of California, Berkeley, Berkeley, CA 94720, USA.

[3] Departments of Microbiology, Immunology, and Molecular Genetics; Pediatrics; and Molecular and Medical Pharmacology, University of California, Los Angeles, Los Angeles, CA 90095, USA.

[4]Integrated DNA Technologies, Coralville, IA, USA

[5]Integrated DNA Technologies, Redwood City, CA, USA

[6]Blood and Marrow Transplant Program, Division of Hematology, UCSF Benioff Children's Hospital Oakland, Oakland, CA 94609, USA

*These authors contributed equally to this work.

**Corresponding authors. Mark Walters: mwalters@mail.cho.org; Jacob Corn: jcorn@berkeley.edu; David Martin: dimartin@chori.org

Sickle Cell Disease (SCD), one of the world's most common genetic disorders, causes anemia and progressive multiorgan damage that typically shortens lifespan by decades; currently there is no broadly applicable curative therapy. Here we show that Cas9 RNP-mediated gene editing with an ssDNA oligonucleotide donor yields more than 20% correction of the sickle mutation in long-term engrafting human HSCs. Using RNA-seq, we further find that *in vivo* erythroid differentiation markedly enriches for cells carrying corrected ß-globin alleles. Adoption of a high-fidelity Cas9 variant demonstrates that this approach can yield efficient editing with almost no off-target events. These findings indicate that the sickle mutation can be corrected in human HSCs at levels that are likely to be curative if translated into a therapy.

SCD (*1*) is an attractive target for correction by gene editing (*2*–*5*) because hematopoietic stem cells (HSCs) can readily be harvested for *ex vivo* manipulation, and SCD is caused by a single point mutation in the ß-globin gene. Our strategy focused on xenografting of human stem and progenitor cells (HSPCs) to assess the edited genotype in the HSCs that drive long-term engraftment, assess the distribution of genotypes among engrafted cells, and examine globin expression in erythroid cells derived from edited HSCs (Figure 1B). Adult human peripheral blood CD34+ HSPCs homozygous for the sickle mutation were obtained by plerixafor mobilization. To correct the sickle mutation (Figure 1A), we electroporated HSPCs with a Cas9 ribonucleoprotein

(RNP)(*6*) targeted to the site of the sickle mutation and a single stranded oligonucleotide donor template programming a wild type *HBB* allele. The only alteration of our previously published protocol (*4*) was the adoption of a synthetic sgRNA with 3xMS protection to improve stability of the guide RNA (3XMS-G10 guide) (*7*). Our oligonucleotide donor facilitates homology-directed repair (HDR) that repairs the cleavage site using the donor sequence as template, alters the PAM sequence to prevent cleavage of the corrected allele, and changes the sickle mutation to the wild type sequence (Figure 1A). After electroporation, cells were injected into NOD.Cg-*Kit*$^{W\text{-}41J}$ *Tyr*$^{+}$ *Prkdc*^{scid} *Il2rg*^{tm1Wjl}/ThomJ (NBSGW) mice, which permit engraftment of human HSCs and erythroid differentiation in the bone marrow (*8*, *9*). 16-20 weeks after injection, we analyzed human cells engrafted in the bone marrow (Figure 1B). We present data on 43 mice in 4 cohorts; mice in each cohort received aliquots of cells from a single electroporation. Human engraftment was robust, (52±27% mean±s.d., Figure 1C; Table S1). Immunophenotyping and colony assays indicated normal lineage potential of the xenografted cells (Figure S1).

We used PCR amplification of the edited region in *HBB*, followed by next-generation sequencing (NGS)(*10*), to quantify editing in xenografted marrows (Figure 1D; Table S1), and found an average of 23.4% of alleles with the corrected genotype, and 65.2% with indels (Figure 1D; Figure S2; Table S1). Previous studies have found substantial NHEJ after long-term engraftment, but a dramatic decline in the proportion of HDR-corrected *HBB* alleles relative to input HSPCs (cells at the time of injection) (*2*, *4*, *5*). Those results have suggested that HSCs carry out homology-directed DNA repair (HDR) less efficiently than the more committed progenitors that make up the majority of cells in the edited HSPC pool. However results in this experiment (Figure 1D) indicate that substantial levels of HDR can be achieved in HSCs.

Mice within the same cohort, despite receiving cells from the same electroporation, exhibit prominent variation in levels of gene correction (Figure 1D; Table S1). To investigate the basis of this variation, we closely examined the alleles present in xenografted marrow. Cas9 cleavage of *HBB* can lead to any of multiple alleles at the edited site: in the absence of HDR, repair by non-homologous end joining (NHEJ) introduces a variety of small insertions or deletions (indels). We used amplicon-NGS to determine the distribution of alleles at both the targeted *HBB* site and at a previously characterized intergenic off-target site (OT1) (*4*, *11*) (Figure 2; Figure S3).

The edited HSPC pools prior to engraftment (“input”) contain a complex assortment of edited alleles. We found that each engrafted mouse carries a unique and smaller set of alleles, consistent with each receiving a discrete but still complex set of stem cells contributing to long-term engraftment. Alleles that are rare in the input population are prominent in some individual mice, but the identity of the prominent alleles differs among the mice (Figure 2; Figure S3). The outsize contribution of these alleles is consistent with some stem cells producing a much higher proportion of marrow cells than others. The observed mouse-to-mouse variation in sickle mutation correction may thus result from each mouse receiving a limited set of stem cells within which the corrected allele was represented to varying degrees, and by individual stem cell clones stochastically contributing disproportionately to the marrow cell population. Our results with gene-edited HSPCs are similar to observations of unique integration sites in lentivirus-transduced HSPCs (*12*, *13*).

We further characterized phenotypic and genotypic correction after engraftment in a subset of mice. Erythrocytes were differentiated *in vitro* from immunoselected marrow CD34+ cells (Figure 3A). They expressed corrected adult ß-globin mRNA and normal adult hemoglobin (HbA), elevated levels of γ-globin mRNA (HBG) and fetal hemoglobin (HbF), and markedly reduced levels of sickle

ß-globin and sickle hemoglobin (HbS) (Figure 3A). To assess the distribution of *HBB* alleles within populations of xenografted cells, we inferred *HBB* genotypes using RNA-Seq data from 359 individual clonal BFU-E colonies derived from marrow CD34+ cells (Figure 3B; Figure S4). This reveals that a substantial proportion of HDR alleles are heterozygous with indel (NHEJ) alleles that are potentially equivalent to ß-thalassemia mutations. Wild type (corrected) *HBB* is dominant over sickle and null (indel) alleles: individuals heterozygous for the sickle mutation, or for a $ß^0$ thalassemia, have functionally normal erythrocytes. The corrected (wild type) alleles in edited HSCs are distributed such that many erythrocytes have only a single wild type *HBB* allele. This distribution produces a proportion of functional erythrocytes that is higher than the proportion of corrected alleles observed in the population of CD34+ cells from which the erythroid colonies were derived (24% functional erythrocytes vs 14.6% corrected alleles). Average gene correction over all xenografted mice (23.4%) was higher than in the subset of mice used for the colony analysis (14.6%), and so the proportion of functional erythrocytes is predicted to be correspondingly higher.

We assessed the effects of *HBB* genotype on the pattern of globin expression in the individual clonal erythroid colonies (Figure 3C). For this analysis, we excluded heterozygous colonies, and separated biallelic indels that alter the reading frame (which are likely to be equivalent to null ß-thalassemia mutations) from biallelic indels that retain the native reading frame. Principal component analysis on expression of the globin genes *HBA*, *HBG*, *HBD*, and *HBB* (Figure 3C, Figure S5) reveals that colonies with out-of-frame indels are skewed toward expression of *HBG*, the fetal ß-like globin gene, while those with in-frame deletions are closer to the pattern of colonies with either sickle or wild type (corrected) *HBB*. This analysis suggests that a large proportion of erythroblasts generated by edited HSCs have a ß-thalassemia phenotype, likely due to out-of-frame indels causing deficiency of *HBB* transcripts along with a proportionally higher contribution of *HBG*.

The findings discussed above (Figure 1, Figure 3B and 3C) indicate that our editing protocol produces a high proportion of indel alleles that are functionally equivalent to ß-thalassemia mutations. But in contrast to ß-thalassemia, after editing HSCs with non-functional *HBB* alleles are mixed with a high proportion of HSCs carrying corrected *HBB* alleles. Deficiency of ß-globin chains leads to apoptosis during late stage erythroid differentiation (“ineffective erythropoiesis”), and a similar phenomenon may occur in sickle cell disease(*14*, *15*). Because cells carrying indels or the sickle mutation on both alleles may be subject to ineffective erythropoiesis, while corrected cells are functionally normal, we asked if erythroid cells in which either one or both *HBB* alleles had been corrected enjoy a selective advantage during erythropoiesis.

NBSGW mice engrafted with human HSCs produce human erythroblasts in their bone marrow (*8*, *9*). We immunoselected human erythroid cells with antibody to CD235a (GlycophorinA), carried out RNA-Seq, and inferred the *HBB* genotypes present in the erythroblast population. For each individual mouse, we compared the proportion of corrected *HBB* alleles in the xenografted bone marrow, in CD34+ cells immunoselected from marrow, and in CD235a+ erythroblasts. To control for enrichment of alleles corrected by HDR, we distinguished two types of HDR: “PAM-only” HDR events mutate the Cas9 PAM without the conversion tract reaching the sickle SNP; whereas “sickle-corrected” HDR events mutate the Cas9 PAM and also correct the sickle SNP (Figure 1A). We observe a marked enrichment of “sickle-corrected” HDR alleles in erythroblasts when compared to marrow or CD34+ cells from the same mouse, but no enrichment of “PAM-only” HDR alleles (Figure 3D, Figure S6). This observed enrichment of corrected *HBB* alleles in edited erythroblasts may reflect the loss of sickle, ß-thalassemia, and sickle/ß-thalassemia cells *in vivo*.

While Cas9 RNP/ssDNA-based gene correction may provide an effective therapeutic option for SCD, wild type Cas9 complexed with the G10 sgRNA exhibits off-target cleavage activity at the previously-characterized site OT1 (*4*, *11*), where an average of 47.5% of alleles have indels after engraftment (Figure S2). While indels at OT1 have no known or predicted deleterious effect, cleavage at other genomic sites has the potential to promote neoplastic progression. To discover and characterize additional potential off-targets, we developed an exhaustive strategy that combines GUIDE-seq (*16*), unbiased off-target identification, bioinformatic searches, and pooled-primer quantification. GUIDE-seq in K562 cells revealed *HBB* and OT1, and an additional five off-target sites; none of the five sites are in a coding region (Figure 4A, Table S2). We term the second-most prevalent of these sites “OT2”. GUIDE-seq in HSPCs found only the OT1 site (Figure S7).

Off-target cleavage may be mitigated by use of recently developed high-fidelity Cas9 variants. We compared targeting of *HBB* and OT1 by RNPs consisting of the 3XMS-G10 guide and WT Cas9, espCas9-1.1(*17*), HF-1(*18*), or Alt-R HiFi Cas9(*19*) in K562 cells (Figure S8) and CD34+ HSPCs (Figure 4B). In K562 cells, all three high fidelity variants reduced off-target editing at both OT1 and OT2. However, HF-1 reduced on-target editing at *HBB* and was therefore not tested further. In HSPCs, only the AltR HiFi variant (IDT) maintained high levels of HDR editing at *HBB* while reducing indel formation at OT1 by ~20-fold, and OT2 by ~10-fold (Figure 4B, Figure S6). We therefore selected the AltR HiFi variant for further study. While indels at OT1 are unlikely to be deleterious, translocations are more of a concern. Translocations between *HBB* and OT1 are detectable in K562 cells and CD34+HSPC edited with wild-type Cas9, but undetectable with AltR HiFi Cas9 using a droplet digital PCR assay(*20*) (Figure 4C). GUIDE-seq with the high-fidelity RNP in K562 cells revealed only *HBB,* OT1, and OT2 (Figure 4D), and GUIDE-seq events were reduced for OT1 and OT2 compared to WT Cas9.

For bioinformatic identification of candidate off-target sites we used CRISPor (*21*), which relies on sequence similarity, and CRISTA (*22*), which relies on machine learning. These tools produced a list of 201 potential off-target sites (Figure 4F). We quantified editing in HSPCs at all 201 sites using a pooled-primer PCR approach capable of simultaneous amplification (*19*). Of all 201 possible off-target sites, wild type Cas9 edited only OT1 and *HBB* in >1% of alleles (Figure 4E, Table S3), but some off-target activity was seen at OT2 (~0.2% of alleles). Alt-R HiFi Cas9 reduced editing at OT1 to 2.1% of alleles, and editing at OT2 was reduced below the limit of detection (from 0.4% to 0.03%, Figure 4E, Table S3). No editing was observed at the 199 other sites with HiFi Cas9. We conclude that, of the 201 potential off-target sites (Figure 4F), only two (OT1 and OT2) are *bone fide* off targets of the wild-type 3xMS-G10 Cas9 RNP, and only one (OT1) is an off-target of the AltR HiFi 3xMS-G10 Cas9 RNP.

Evidence from mixed donor chimerism after allogeneic hematopoietic stem cell transplantation for SCD and ß-thalassemia indicates that that as little as 10% (SCD) or 20% (ß-thalassemia) of wild-type donor cells are sufficient to render a recipient free of disease, because functional erythrocytes (carrying at least one wild type *HBB* allele) have a selective advantage during erythropoiesis and in circulation (*23*–*26*). We observe robust marrow engraftment of edited HSCs, correction of the sickle mutation in more than 20% of ß-globin alleles, evidence that cells carrying the corrected allele enjoy a competitive advantage during erythroid differentiation *in vivo*, and little evidence of off-target editing by the Cas9 RNP. This protocol may thus form the basis of a therapy based on correction of the sickle mutation in autologous HSCs.

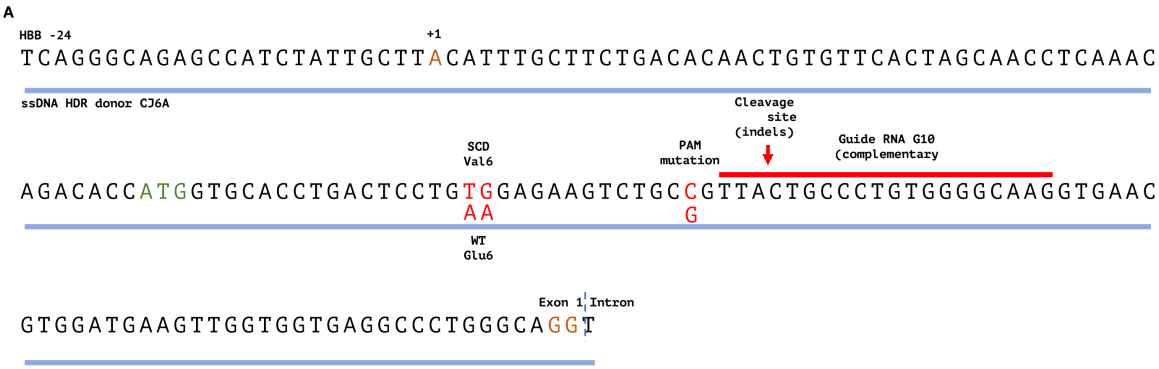

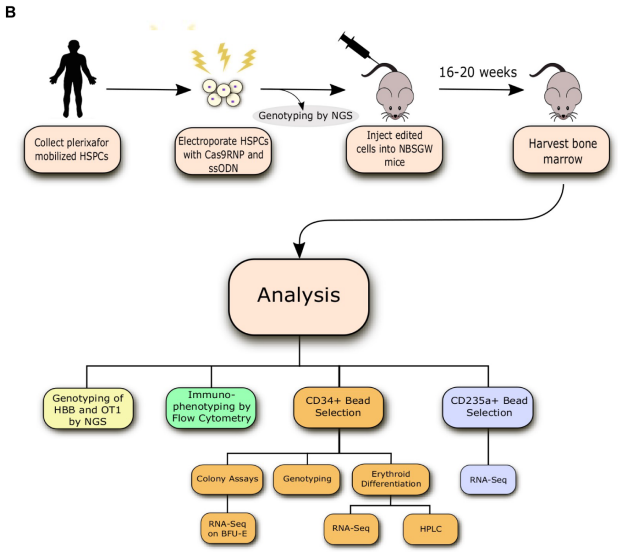

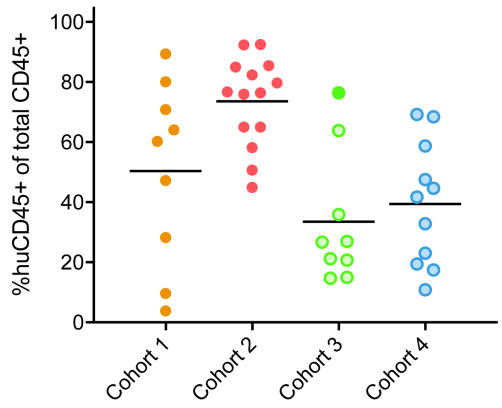

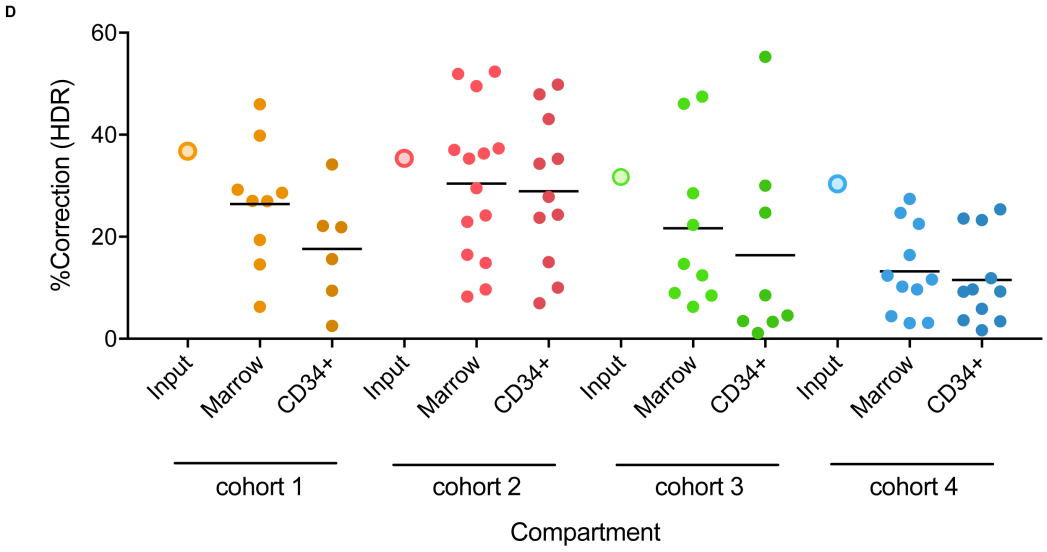

Figure 1. Correction of the sickle mutation in long-term xenografted hematopoietic cells. A) Schematic depicting targeting of the sickle mutation with the G10 guide RNA (in red) and the single-stranded DNA oligonucleotide donor CJ6A (blue). Sequence changes induced by the donor are shown in red; HDR proceeds from the Cas9 cleavage site (red arrow) but does not always extend to the site of the sickle mutation. B) Schematic outlining the large-scale xenografting experiment, and analysis of the engrafted cells. C) Engraftment of human hematopoietic cells in mouse bone marrow at 16-20 weeks post-injection, assessed by flow cytometry and displayed as percent of total marrow hematopoietic cells. D) Correction of the sickle mutation in xenografted marrow cells, and marrow CD34+ cells, at 16-20 weeks post-injection, expressed as percent of *HBB* alleles. The horizontal line denotes the average correction in each group; Input (large open circles) denotes percent correction in the pool of edited cells injected into each cohort.

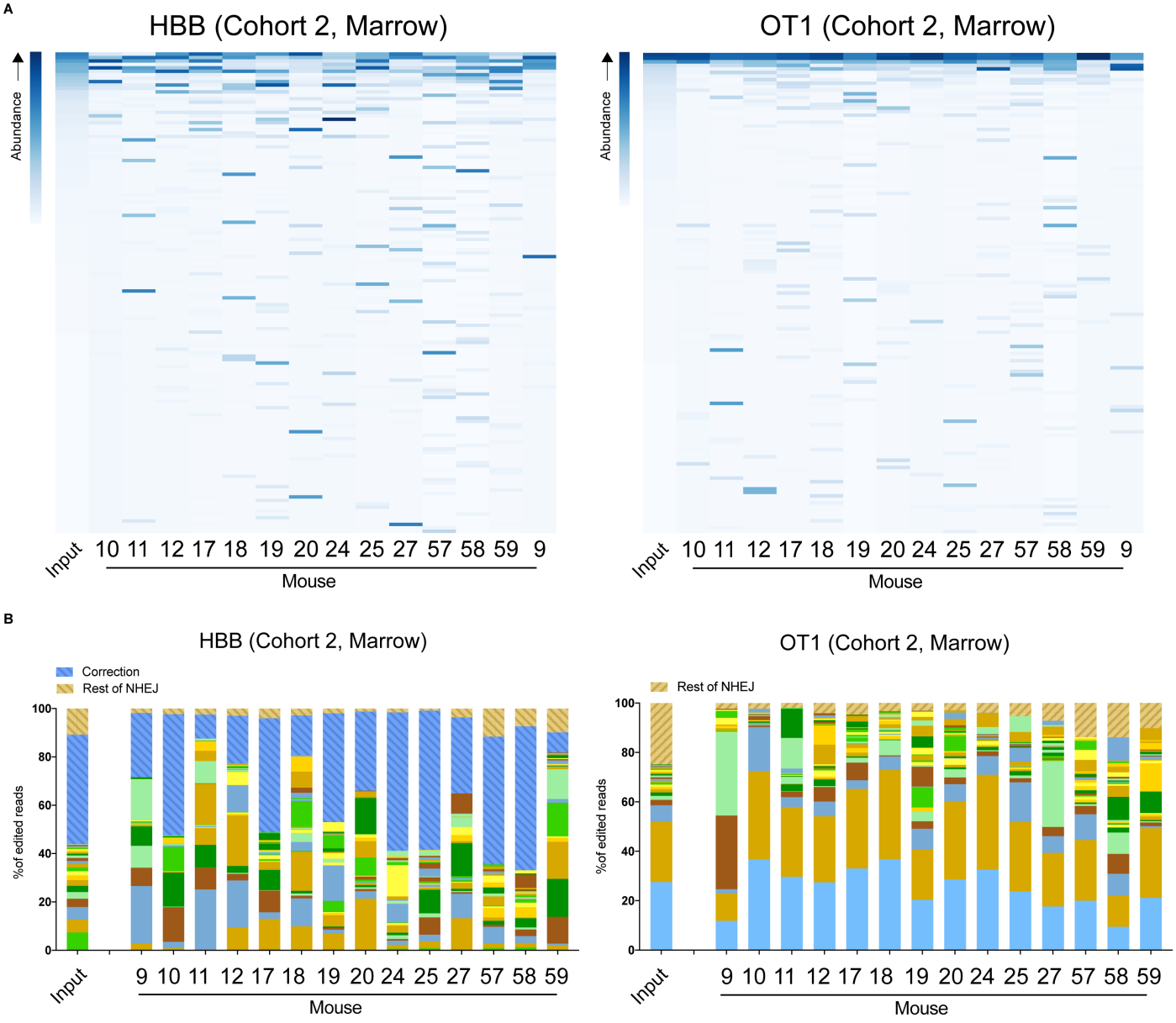

Figure 2. **Analysis of allelic diversity in edited and xenografted hematopoietic cells**. A) Heatmaps of abundance of alleles (rows) in input sample (first column) versus xenografted mice. Alleles are sorted (vertically) by decreasing abundance in the input sample, and filtered for alleles with at least 0.1% abundance in some mouse or the input, resulting in 140 HBB and 135 OT1 alleles. Note that the most common alleles in the input population are of minor abundance in some mice, while alleles that are rare in the input may be common in one or more mice. B) Stacked bar graphs indicating the contribution of the top 24 indel alleles (solid bars) at *HBB* (left) and OT1 (right) in each Cohort 2 mouse, as a fraction of all aligned and edited reads. All other NHEJ alleles

are contained in brown striped bars (top segment); the corrected *HBB* alleles (HDR) are shown as a blue striped bar (second segment from top).

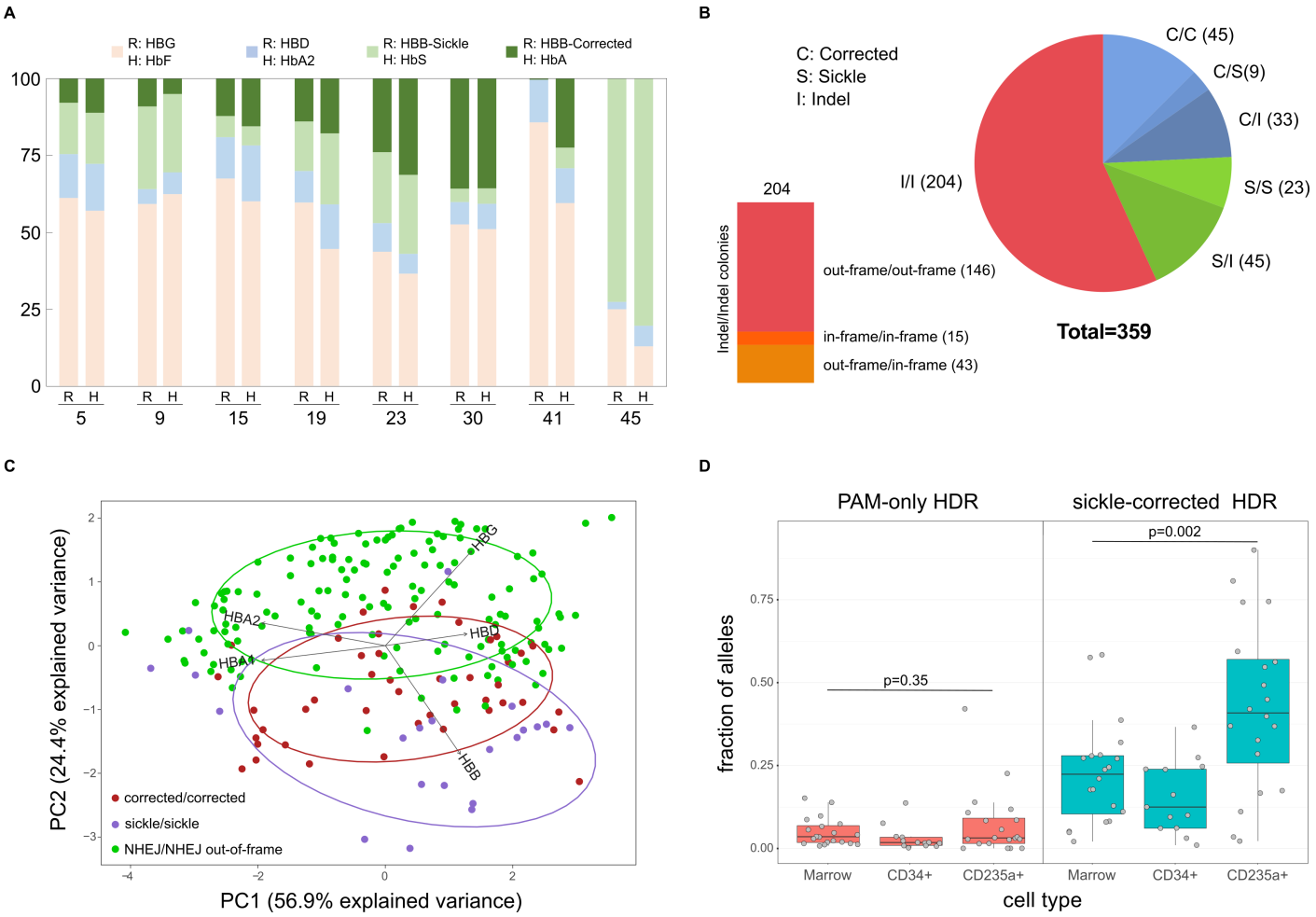

Figure 3. Globin expression, allelic assortment, and *in vivo* selection for corrected HBB genotype in erythroid cells. A) RNA-Seq (R) and HPLC (H) on erythrocytes differentiated from CD34+ marrow cells of 8 xenografted mice; mouse 45 was engrafted with unedited cells. For RNA-Seq, only ß-like globins are shown, in colors matching the corresponding hemoglobin assayed by HPLC. Note the prominent decline in sickle mRNA and hemoglobin in edited cells, and the marked increase in fetal (γ) globin and fetal hemoglobin (HbF). B) Assortment of genotypes inferred from RNA-Seq of clonal erythroid colonies differentiated from xenografted marrow CD34+ cells, with homozygous NHEJ colonies further characterized by in- vs. out-of-frame deletions in the bar at left. 24% of CFU harbored at least one corrected allele. C) Principal component analysis of RNA-seq data from erythroid colonies with homozygous genotypes; dots represent individual colonies, and ellipses encompass 68% of colonies of each type. Colonies with out-of-frame indels at *HBB* have a reduced ratio of *HBB* to *HBG* mRNA. Principal component analysis of colonies with in-frame indels is shown in Figure S5. D) Comparison of the distribution (box plot) of HDR allele frequency in total marrow and marrow CD34+ genomic DNA, and marrow erythroid (CD235+) cell RNA; data for individual mice are shown as circles. A “sickle-corrected” HDR allele has both the PAM mutation and sickle correction, while a “PAM-only” HDR allele has the PAM mutation but no sickle correction. The corrected allele is enriched in erythroid cells compared to the PAM-only allele; for a line plot showing individual mice see Figure S6.

A

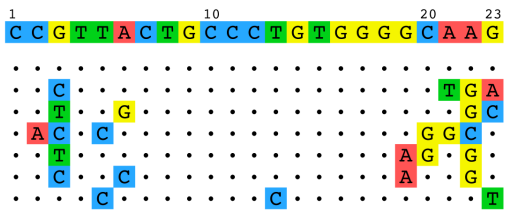

	Replicate 1	Replicate 2	Replicate 3
chr11:5226984 (HBB)	x	x	x
chr12:93155425	x	x	x
chr12:124319288 (OT2)	x	x	x
chr17:78243561	x	x	
chr19:33890031	x		x
chr9:101833600 (OT1)	x	x	x
chr17:68628105		x	x
chr12:132288220			x

B

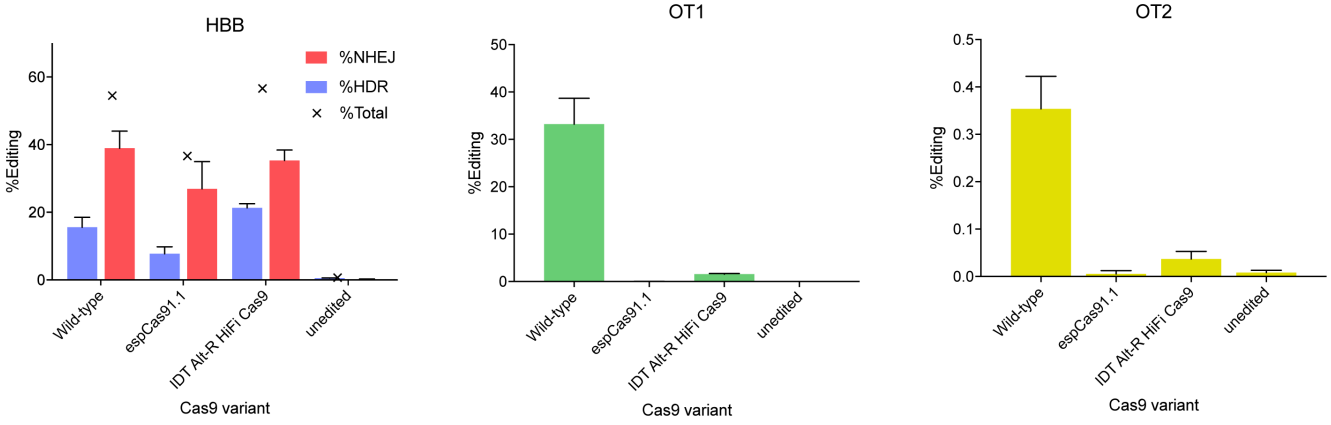

C

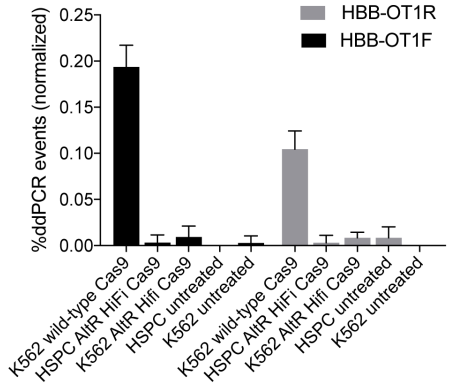

D

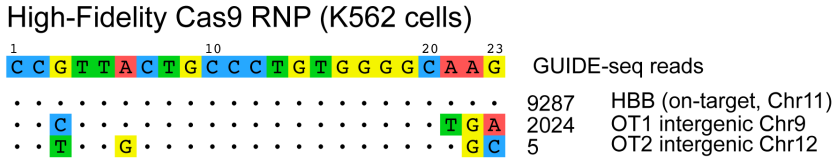

E

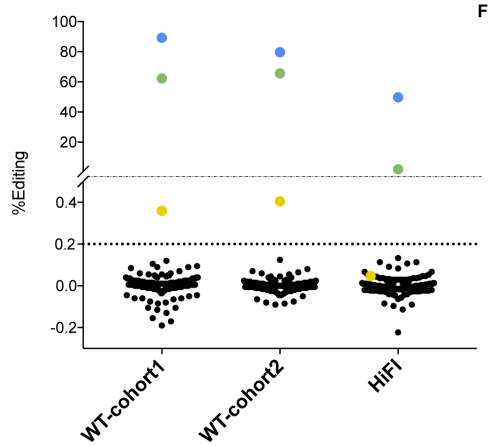

F

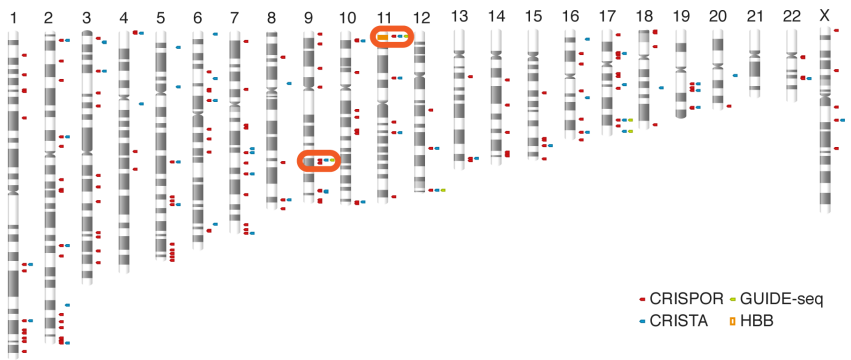

Figure 4. **Assessment of off-target cleavage in the Cas9 RNP/ssDNA gene correction protocol**. A) Representative GUIDE-seq result with the Cas9 RNP in K562 cells (left) and a table (right) depicting the GUIDE-seq hits detected in three independent replicates. B) Comparison of high-fidelity Cas9 variants espCas9-1.1 (*19*) and HF-1 (*18*) in editing at *HBB* in healthy donor CD34+ HSPC. C) Translocations between HBB and OT1 are apparent on a droplet digital PCR (ddPCR) assay when wild-type Cas9 is used to target *HBB*, but not when Alt-R HiFi Cas9 is used, as measured by ddPCR detection of translocation products formed from the region upstream of *HBB* and either the region upstream of OT1 (OT1F) or the region downstream (OT1R). D) Representative GUIDE-seq result using the Alt-R HiFi Cas9 RNP in K562 cells or healthy donor CD34+ HSPC. Only OT1 and OT2 are detected. E) Total gene editing rates (%HDR + %NHEJ) measured by pooled-primer PCR at 190 of 201 identified off-targets, assayed in the edited sickle CD34+ HSPCs injected into Cohorts 1 and 2 (“input” in Figure 1C and Figure 2), as well as healthy donor CD34+ HSPC separately edited with Alt-R HiFi Cas9, with indels observed at the same sites from untreated cells subtracted. Blue dots: on-target *HBB*; green dots: off-target OT1; yellow dots: off-target OT2. Only OT1 and OT2 are edited at >0.2% (lower dashed line) of alleles by wild-type Cas9, and only OT1 by high-fidelity Cas9. F) Genome decoration schematic depicting off-target sites identified by GUIDE-seq, CRISTA, and CRISPor, with the sites with actual editing detected (>0.2% of alleles using high-fidelity Cas9) indicated with a red box.

References

1. F. B. Piel, M. H. Steinberg, D. C. Rees, Sickle Cell Disease. *New England Journal of Medicine*. **376**, 1561–1573 (2017).

2. M. D. Hoban *et al.*, *Blood*, in press, doi:10.1182/blood-2014-12-615948.

3. M. D. Hoban *et al.*, CRISPR/Cas9-Mediated Correction of the Sickle Mutation in Human CD34+ cells. *Molecular Therapy*. **24**, 1561–1569 (2016).

4. M. A. DeWitt *et al.*, Selection-free genome editing of the sickle mutation in human adult hematopoietic stem/progenitor cells. *Science Translational Medicine*. **8**, 360ra134-360ra134 (2016).

5. D. P. Dever *et al.*, CRISPR/Cas9 β-globin gene targeting in human haematopoietic stem cells. *Nature*. **539**, 384–389 (2016).

6. S. Lin, B. Staahl, R. K. Alla, J. A. Doudna, Enhanced homology-directed human genome engineering by controlled timing of CRISPR/Cas9 delivery. *eLife*. **3**, e04766 (2014).

7. A. Hendel *et al.*, Chemically modified guide RNAs enhance CRISPR-Cas genome editing in human primary cells. *Nature Biotechnology*. **33**, 985–989 (2015).

8. B. E. McIntosh *et al.*, Nonirradiated NOD,B6.SCID Il2rγ−/− KitW41/W41 (NBSGW) Mice Support Multilineage Engraftment of Human Hematopoietic Cells. *Stem Cell Reports*. **4**, 171–180 (2015).

9. C. Fiorini *et al.*, Developmentally-faithful and effective human erythropoiesis in immunodeficient and *Kit* mutant mice. *American Journal of Hematology*. **92**, E513–E519 (2017).

10. L. Pinello *et al.*, Analyzing CRISPR genome-editing experiments with CRISPResso. *Nature Biotechnology*. **34**, 695–697 (2016).

11. T. J. Cradick, E. J. Fine, C. J. Antico, G. Bao, CRISPR/Cas9 systems targeting β-globin and CCR5 genes have substantial off-target activity. *Nucleic acids research*. **41**, 9584–92 (2013).

12. K. Ronen *et al.*, Distribution of lentiviral vector integration sites in mice following therapeutic gene transfer to treat β-thalassemia. *Molecular therapy : the journal of the American Society of Gene Therapy*. **19**, 1273–86 (2011).

13. A. Biffi *et al.*, Lentiviral vector common integration sites in preclinical models and a clinical trial reflect a benign integration bias and not oncogenic selection. *Blood*. **117**, 5332–9 (2011).

14. J.-A. Ribeil *et al.*, Ineffective Erythropoiesis in β-Thalassemia. *The Scientific World Journal* (2013), , doi:10.1155/2013/394295.

15. C. J. Wu *et al.*, Evidence for ineffective erythropoiesis in severe sickle cell disease. *Blood*. **106**, 3639–45 (2005).

16. S. Q. Tsai *et al.*, GUIDE-seq enables genome-wide profiling of off-target cleavage by CRISPR-Cas nucleases. *Nature biotechnology*. **33**, 187–197 (2014).

17. I. M. Slaymaker *et al.*, Rationally engineered Cas9 nucleases with improved specificity. *Science*. **351**, 84–88 (2016).

18. B. P. Kleinstiver *et al.*, High-fidelity CRISPR–Cas9 nucleases with no detectable genome-wide off-target effects. *Nature*. **529**, 490–495 (2016).

19. C. A. Vakulskas *et al.*, A high-fidelity Cas9 mutant delivered as a ribonucleoprotein complex enables efficient gene editing in human hematopoietic stem and progenitor cells. *Nature Medicine*. **24**, 1216–1224 (2018).

20. J. Long *et al.*, Characterization of Gene Alterations following Editing of the β-Globin Gene Locus in Hematopoietic Stem/Progenitor Cells. *Molecular therapy : the journal of the American Society of Gene Therapy*. **26**, 468–479 (2018).

21. M. Haeussler *et al.*, Evaluation of off-target and on-target scoring algorithms and integration into the guide RNA selection tool CRISPOR. *Genome Biology*. **17**, 148 (2016).

22. S. Abadi, W. X. Yan, D. Amar, I. Mayrose, A machine learning approach for predicting CRISPR-Cas9 cleavage efficiencies and patterns underlying its mechanism of action. *PLoS computational biology*. **13**, e1005807 (2017).

23. M. C. Walters *et al.*, Stable mixed hematopoietic chimerism after bone marrow transplantation for sickle cell anemia. *Biol Blood Marrow Transplant*. **7**, 665–73 (2001).

24. C. D. Fitzhugh *et al.*, At least 20% donor myeloid chimerism is necessary to reverse the sickle phenotype after allogeneic HSCT. *Blood*. **130**, 1946–1948 (2017).

25. R. Iannone *et al.*, Results of minimally toxic nonmyeloablative transplantation in patients with sickle cell anemia and beta-thalassemia. *Biol Blood Marrow Transplant*. **9**, 519–28 (2003).

26. M. Andreani *et al.*, Quantitatively different red cell/nucleated cell chimerism in patients with long-term, persistent hematopoietic mixed chimerism after bone marrow transplantation for thalassemia major or sickle cell disease. *Haematologica*. **96**, 128–133 (2011).

27. M. A. DeWitt *et al.*, Selection-free genome editing of the sickle mutation in human adult hematopoietic stem/progenitor cells. *Science Translational Medicine*. **8**, 360ra134 (2016).

28. S. Lin, B. Staahl, R. K. Alla, J. A. Doudna, Enhanced homology-directed human genome engineering by controlled timing of CRISPR/Cas9 delivery. *eLife*. **3**, e04766 (2014).

29. S. Picelli *et al.*, Smart-seq2 for sensitive full-length transcriptome profiling in single cells. *Nature methods*. **10**, 1096–8 (2013).

30. N. L. Bray, H. Pimentel, P. Melsted, L. Pachter, Near-optimal probabilistic RNA-seq quantification. *Nat Biotech*. **34**, 525–527 (2016).

31. B. Langmead, S. L. Salzberg, Fast gapped-read alignment with Bowtie 2. *Nat Methods*. **9**, 357–9 (2012).

32. E. Garrison, G. Marth, Haplotype-based variant detection from short-read sequencing (2012) (available at http://arxiv.org/abs/1207.3907).

33. S. Abadi, W. X. Yan, D. Amar, I. Mayrose, A machine learning approach for predicting CRISPR-Cas9 cleavage efficiencies and patterns underlying its mechanism of action. *PLoS computational biology*. **13**, e1005807 (2017).